Low-Mass Pre–Main Sequence Stars and Their X-ray Emission

Ralph Neuhäuser

To investigate the formation and early evolution of stars, astronomers study the x-ray emission of T Tauri stars, which are young, solar-mass stars called pre–main sequence stars. Two Earth-orbiting x-ray satellites, the Röntgen X-ray Satellite (ROSAT) and the Advanced Satellite for Cosmology and Astrophysics (ASCA), have discovered x-ray emission from young protostars, called Class I objects. Many T Tauri stars were detected as x-ray sources by ROSAT. X-ray luminosity functions and correlations with other stellar parameters can be studied and used to investigate the x-ray emission mechanism. From the ROSAT data hundreds of T Tauri stars have been discovered, some of which are located outside regions of ongoing star formation. Stellar x-rays also irradiate circumstellar disks, regions where planets may form, so x-ray emission data from T Tauri stars may also be used to investigate the formation of planets.

Stars are born during the collapse of gas and dust clouds, so the youngest protostars are best observed at infrared (IR) and millimeter wavelengths (*1*). Optical emission from the protostar is absorbed in the dense circumstellar environment, but x-rays can penetrate the dense clouds. As the protostar evolves, the circumstellar envelope clears, aiding the detection of optically visible young stars. One can learn about the evolution of a star by placing it into the Hertzsprung-Russell (HR) diagram (*2*). Normal stars line up in the HR diagram on the main sequence (MS). From the location of a star in this diagram, one can estimate its age, mass, and radius.

Stars with masses less than ~3 $M_\odot$ (with 1 $M_\odot$ = 2 × 10^{33} g = mass of the sun) are regarded as low-mass stars and have late spectral types, namely G, K, or M (*2*), equivalent to low surface temperatures of ~3500 to 6000 K. Such stars are also called late-type stars. Young, low-mass stars have large surface areas, with their radii being up to several times larger than the radius of our sun ($R_\odot$ = 7 × 10^5 km). A star with a large surface area has high luminosity and occurs above the MS in the HR diagram if it has low surface temperature(Fig. 1). Such stars are called pre-MS stars. They are still contracting, so they evolve downward to the MS as their luminosity and effective temperature (T_{eff}) decrease. As soon as a star has reached the MS, its energy is supplied by steady hydrogen burning. Stars just reaching the MS, like those of the Pleiades cluster that are ~10^8 years old, define the zero-age main sequence (ZAMS). Low-mass stars spend several billion years on the MS and then evolve from the MS upward as their radii and luminosities increase.

The major physical difference between low-mass pre-MS and MS stars is their energy sources. Pre-MS stars gain gravitational energy from contraction, whereas the main energy source of MS stars, like the sun, is the steady burning of hydrogen. The evolution of a star to the MS reflects variations in the star's interior. The time scale and physics of the evolution of a star depends on the mass of the star. Stars with masses larger than ~8 $M_\odot$ have essentially no pre-MS phase, because they are burning hydrogen by the time protostellar accretion has ended, after ~10^5 years. Presumably, they form within massive, dense cloud cores, so that their collapse and evolution proceed faster than in low-mass stars. Intermediate-mass stars (Herbig Ae/Be stars) in their pre-MS phase evolve more slowly and reach the MS after ~10^6 years (*3*). Young, low-mass, pre-MS stars are called T Tauri stars (TTS), named after the prototype, star T in Taurus. TTS need several million years to reach the MS. They have spectral types F6 (corresponding to ~3 $M_\odot$ on the MS) to late M (~0.08 $M_\odot$).

Stars are made up of plasma, and even though the surface of a late-type star has a temperature of only several thousand kelvin, the material is much hotter inside the star and exceeds 10^7 K. The outer convection zone is a thin sphere in our sun, but this zone is thicker in TTS. In a rapidly rotating star, magnetic field lines can also be twisted by a dynamo, which effectively perturbs and strengthens the magnetic field (*4*). Dark spots optically visible on the stellar surface are small regions where magnetic field lines emerge from the stellar surface. Pairs of dark spots are sometimes connected by loops that contain plasma—hot material ejected from the star—which heats up to ~10^7 K and emits x-rays. This x-ray emission is line emission from hot, optically thin plasma and, in some parts, it is thermal bremsstrahlung. X-ray flares are observed, which also indicate magnetic energy release. X-ray emission of TTS is due to solarlike magnetic activity, but x-ray luminosities for TTS are ~10^3 times as large as the x-ray luminosity of the sun (*5*).

The angular momentum evolution of low-mass stars, one of the major problems in our understanding of the pre-MS phase, can be studied indirectly with x-ray observations under the assumption that a stellar dynamo is responsible for the x-ray emission. The faster the star rotates, the stronger the x-ray emission should be. In addition, there is a correlation between thermal x-ray and nonthermal radio emission in late-type stars. Both types of emissions and their correlation are indirect evidence for magnetic fields and the dynamo effect.

Low-mass stars begin their life rotating relatively slowly, with rotation periods of less than 10 days. Then, their rotation increases significantly, and some stars reach the ZAMS with rotation periods of less than a day. Later on in the MS their rotation decreases. Rotational velocities can be measured spectroscopically from line broadening. Hot and cool spots found on the surfaces of TTS cause photometric variability and can be used to derive the rotation period of the star (*6*).

Here, I will review the basic properties of TTS and their evolution toward the MS. Important advances in the study of TTS have been made in the past decade, including the confirmation of the Kant-Laplace nebula hypothesis, by the discovery of circumstellar disks around many low-mass stars (*7, 8*). ROSAT pointed observations led to the discovery of x-ray emission from young protostars (Class I objects). The spatially complete ROSAT All-Sky Survey (RASS) observations have enabled us to investigate the x-ray emission mechanism by studying luminosity functions and correlations between x-ray emission and other stellar parameters such as rotation. Also, RASS led to the discovery of hundreds of young stars, most of which are TTS associated with star-forming clouds. The others are young ZAMS stars partly concentrated toward the Gould Belt, or other active ZAMS stars that are found anywhere in the sky and are distributed symmetrically around the galactic plane.

Low-Mass, Pre–Main Sequence Stars

Star formation in the galaxy can best be investigated by observing nearby star-forming regions (SFRs). Members of a particular

Max-Planck-Institut für extraterrestrische Physik, D-85740 Garching, Germany. E-mail: rne@mpe-garching.mpg.de

SFR form a homogeneous set of young stars. They share about the same age and distance from Earth but show a range in mass. One of the best studied SFRs is the nearby Taurus SFR at a distance of 140 parsec (pc) (*9*). There are SFRs such as the Chamaeleon SFR where apparently only low-mass stars ($\leq 3\ M_\odot$) are born. Other SFRs, so-called OB associations such as the Orion SFR, contain high-mass stars ($\sim$8 to 100 $M_\odot$), which have spectral types O and B (*2*), as well as many low-mass stars. SFRs often show a filamentary dark cloud structure, and the gas and dust in OB associations is illuminated by their high-mass stars. An SFR without any high-mass stars is called a T association. Most members of a T or OB association share the same kinematics, that is, radial velocity (motion toward or away from the sun) and proper motion (motion projected on the sky). Although conventional methods of searching for TTS are usually spatially restricted to known star-forming clouds, a few isolated TTS were known before the first sensitive all-sky surveys for TTS with the InfraRed Astronomy Satellite (IRAS) and ROSAT; these TTS are isolated in the sense that they are located far from clouds (*10*).

The pre-MS phase, the formation and early evolution of a low-mass star from the initial cloud collapse through the T Tauri phase until the ZAMS (Fig. 1), can be described by following the evolution of the young sun on its way through the HR diagram. Stars form in giant molecular cloud complexes that are typically as large as 100 pc (1 pc = 3×10^{13} km), have densities of $\sim$100 particles per cubic centimeter, and have a temperature of $\sim$20 to 100 K. Because of nonuniform density distributions within cloud complexes, small and dense cloud cores can form. A cloud will collapse under its own gravity if critical conditions are fulfilled (*1*). When a massive cloud collapses, it can fragment and form multiple protostellar systems (*11*).

A protostar remains embedded in a cloud and continues to accrete cloud material. Such an object has a spectral energy distribution with positive slope (*1*). The positive slope $n > 0$ means that much more emission is observed at the IR and submillimeter and millimeter wavelengths than at the optical wavelength. It was suggested (*12*) that n be used to define different classes of young stars: In the resulting classification, Class I objects are $\sim 10^5$-year-old protostars in the accretion phase with $n > 0$. The Class I object is optically invisible (*13*) because there is an optically thick circumstellar envelope (Fig. 2A) surrounding it.

The location in the HR diagram where Class I protostars become optically visible objects (Fig. 1) defines the birthline (*14*), and the protostars become Class II objects, or classical TTS (cTTS) (Fig. 2B), with $n \cong 0$ to -1.5. Now, the star contracts and on the HR diagram moves toward the MS. Energy transport inside the star is dominated by convection, hence this part of the track of the star toward the MS is called the convective track (Fig. 1).

Because of angular momentum conservation during collapse of the cloud, a circumstellar disk develops in the equatorial plane of the protostar (Fig. 2B), and remaining material from the circumstellar envelope accretes onto this disk instead of falling onto the protostar. Further accretion by the protostar comes from the disk and is channeled through funnel flows (*15*). Observational evidence for circumstellar material is derived mainly from excess emission in IR and millimeter wavelengths. Emission from material colder than the stellar photosphere in excess of a hot, stellar blackbody spectrum is observed in many cTTS (*7*). Observations with the Hubble Space Telescope (HST) resolved circumstellar disks (*7, 8*) with typical sizes of 1.5×10^{10} km, a few hundred times the distance between Earth and the sun.

Hundreds of cTTS have been found in many different SFRs (*16*). All of them exhibit Balmer lines, like hydrogen Hα at 6563 Å, and the Fraunhofer calcium H and K emission lines (Ca H and K). Also, many of these cTTS display ultraviolet (UV) and IR emission in excess of a hot blackbody (*7*). Their ages range from $\sim 10^5$ to a few million years.

There should be many more evolved TTS (*17*) if star formation can last as long as the age of the cloud complex, typically several 10^7 years. However, such post-TTS would be difficult to observe because of their reduced activity. A lithium (Li) survey could detect such post-TTS. The presence of the Li absorption line at 6708 Å can serve as a reliable youth indicator, because it is quickly depleted by (p,α) proton capture processes in convective envelopes that extend sufficiently deep into a cool star such that the Li fusion temperature of $\sim 2.5 \times 10^6$ K is reached (*18*). Because G- and K-type ZAMS stars also show some Li absorption, one has to measure the Li abundance precisely to classify a young star as either a ZAMS or a pre-MS star.

A search for such post-TTS had been undertaken with the Einstein Observatory x-ray satellite (EO). Optical follow-up observations of unidentified EO sources led to the discovery of many TTS with weak Hα and IR excess emission (*19, 20*). These weak-line TTS (wTTS) (Fig. 2C) turned out to be the dominant population among TTS. The conventional dividing line between cTTS and wTTS is at an Hα equivalent width (that is, the line strength) of W_λ (Hα) = 10 Å, but this is somewhat arbitrary because for a given Hα flux, W_λ depends on the spectral type. The observed Hα flux would be a better discriminator between TTS with and without accretion disks (*20*).

The angular momentum of a cTTS may be regulated by the disk through an anchoring effect (*21*). The stellar magnetic field anchors with the magnetic field of the disk. At the distance from the star where this interaction has taken place, the disk rotates more slowly than the star itself; hence, the disk-star anchoring effectively slows down the stellar rotation. Only after the disk dissipates can the star continue to increase its rotation, so TTS without disks should rotate faster. Observations confirm that wTTS rotate faster than cTTS (*4*).

Because wTTS are much more widely distributed in space than cTTS and because in wTTS accretion is coming to a halt, it

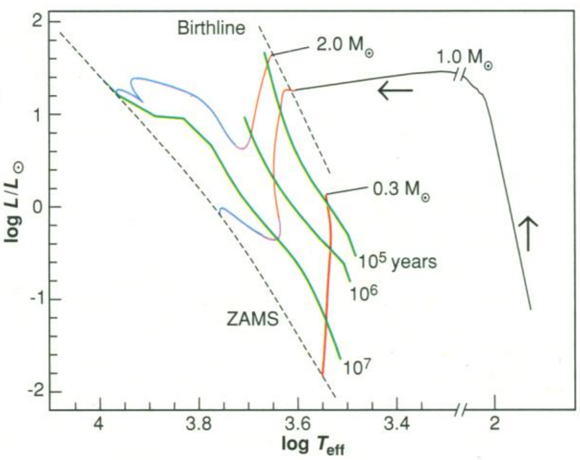

Fig. 1. The location of a star in the HR diagram, a plot of stellar luminosity log $L/L_\odot$ versus effective temperature log $T_{\rm eff}$ ($T_{\rm eff}$ is in kelvin), indicates its evolutionary status. The tracks of three stars with different masses of 0.3, 1.0, and 2.0 $M_\odot$ (mass when accretion stopped) are shown. A star begins its life as a cold protostar. Accretion of material onto the star leads to an increase in size and, consequently, luminosity. As soon as it reaches the birthline (*14*), it can be seen optically. Then, the star contracts down along a convective track (red curve). As soon as a radiative core develops in its center, it turns onto the radiative track (blue curve). Finally, it reaches the ZAMS. Theoretical isochrones (green curves with ages) and pre-MS tracks (black, red, and blue curves) are taken from (*23*).

was suggested that wTTS are identical to post-TTS, or even to sunlike stars possibly having orbiting planets (Fig. 2D). This would be in agreement with the standard model of low-mass star formation (*1*) in which cloud collapse is regulated by ambipolar diffusion (ion drift) and is followed by a phase with strong stellar winds or disk winds (or both) and a circumstellar accretion disk (cTTS). Later on, the disk material disperses or accretes into larger bodies, resulting in a TTS without an active disk (wTTS). This standard model is only valid for single TTS, but recent observations have shown that most TTS are binary stars (Fig. 2E), which can form by capture, by fragmentation of a disk, or from a collapsing filamentary cloud (*22*).

For the EO-discovered wTTS to be the expected post-TTS, they would have to be older than cTTS and located closer to the ZAMS in the HR diagram. As soon as a radiative core has developed and energy transport by radiation is more efficient, a star turns from the convective track to the radiative track (Fig. 1). Its spectral energy distribution is that of a hot blackbody. Such a star is called a Class III object ($n \simeq -2$ to -1.5) and has either an optically thin disk or no disk (Fig. 2C). Because wTTS were found not only on radiative tracks but also on convective tracks, the wTTS population is distinct from the proposed post-TTS population.

To find out whether a wTTS is either on the convective or radiative track, one needs to place the star in the HR diagram and therefore needs to know its distance from Earth. This is usually not a problem for TTS in SFRs, as their distances are relatively well known. However, for an isolated TTS, the distance can be deduced only from the parallax, which can be determined precisely only for stars closer than ~100 pc (*9*). The age and mass of a TTS can be estimated by comparing its location in the HR diagram with theoretical isochrones and evolutionary tracks, which are model-dependent (*23*). Although such models may not give precise absolute ages and masses, they should yield correct relative ages and masses.

X-ray Emission from Protostars

The interstellar material is as translucent for x-rays at 1 keV as for near-IR photons at ~2 μm (*24, 25*) but much less translucent for optical light; hence, x-rays can be used to look as deep into a star-forming cloud as in the near-IR. ROSAT (*26*) and ASCA (*27*) can detect x-rays from deeply embedded objects and offer an alternative approach for investigating the earliest phases of low-mass star formation.

Several Class I objects were found close to x-ray sources in a deep ROSAT positional sensitive proportional counter (PSPC) pointed observation of the young and compact SFR ρ Ophiuchi (ρ Oph) (*24*). Because of source confusion, their identification was ambiguous, but one source (YLW15 = IRS43) was confirmed by a recent ROSAT HRI observation (*28*). With ASCA, several Class I objects belonging to the Coronet Cluster in the SFR around star R in Corona Australis (CrA) were detected (*29*). Three Class I x-ray detections in CrA were confirmed with ROSAT (*30*) (Fig. 3). Another

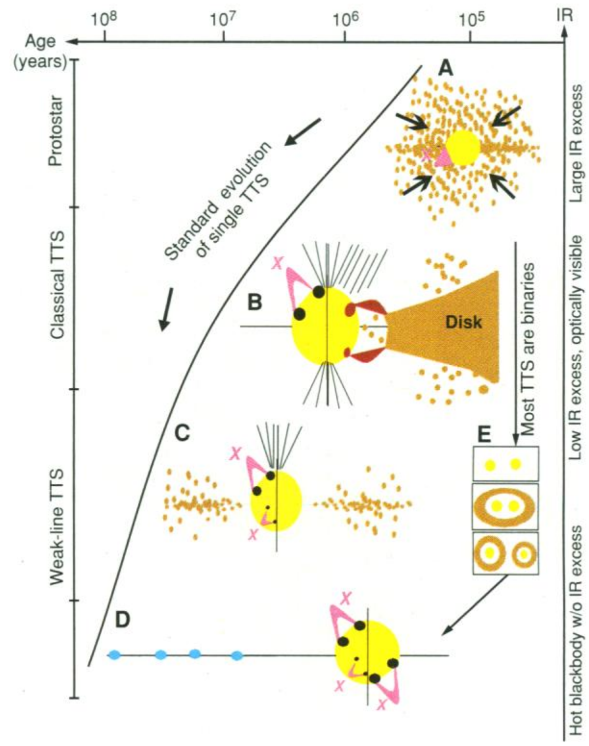

Fig. 2. Schematic model of low-mass stellar evolution including TTS and their x-ray emission. The IR excess emission increases from the bottom to the top, the age from the right to the left (w/o, without). (**A**) A collapsing cloud core forms a Class I protostar, shown as a yellow circle. Cloud material, represented by orange circles, is in-falling (black arrows), and a circumstellar disk in the mid-plane forms. Plasma sheets shown in pink emit x-rays indicated by the pink X. (**B**) A classical TTS with a circumstellar disk produces strong winds, indicated by black lines near the stellar poles. Accretion by funnel flow, shown as red regions to the right of the protostar, is continuous and produces hot spots (red circles) on the stellar surface. Magnetic loops emerge from the stellar surface, producing dark spots (black circles), which are connected by hot plasma loops (pink curves) that emit x-rays. The circumstellar disk and funnel flows surround the whole star in its equatorial plane, and winds are blown away from the northern and southern poles and probably also from the disk. (**C**) Weak-line TTS have only dark spots but stronger x-ray emission than classical TTS, and they have shallow or no disks. The wTTS winds are also blown away from both poles and maybe also from the disk, if it is still present. (**D**) The final stage of low-mass pre-MS evolution is a naked TTS evolving into a sunlike star possibly with orbiting planetesimals or planets (blue circles). (**E**) Most TTS, however, are binaries, so that some TTS may be born without a disk or have a short-lived disk. There exist binaries without disks (top panel), with circumstellar disks (middle panel), and with circumbinary disks (bottom panel).

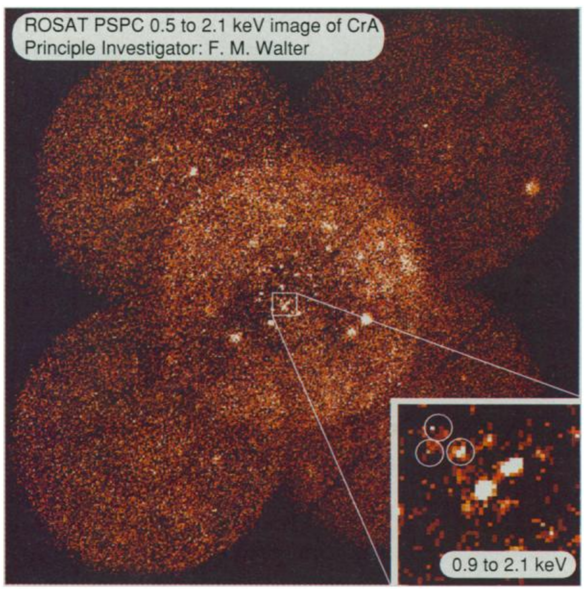

Fig. 3. Combined image of five ROSAT PSPC pointed observations of R CrA and its surroundings in the range of 0.5 to 2.1 keV. X-ray–emitting TTS and Class I objects are visible as pointlike sources in the center. The PSPC field of view has a 2° diameter. (**Inset**) Central area of the pointed observation in the range of 0.9 to 2.1 keV with three Class I protostar x-ray sources circled.

Class I object, SVS16 in the compact SFR NGC 1333 in Perseus, was detected in a ROSAT HRI observation (*31*).

Because Class I objects are deeply embedded in clouds, most of their faint x-ray emission is absorbed close to the star, making an estimation of the star's x-ray luminosity, L_X, difficult. The ASCA and ROSAT detections yield $L_X \simeq 10^{30}$ to 10^{31} erg s^{-1} in the 0.1- to 2.4-keV range for the Class I objects in CrA (*29, 30*), similar to YLW15 in ρ Oph and SVS16 in NGC 1333 (*26, 31*). One of the ASCA sources (probably IRS 7) showed a powerful x-ray flare. During the flare, the peak x-ray emission energy was at 6 keV, indicating a plasma as hot as $\sim 10^8$ K (*29*). The ROSAT HRI observation of YLW15 in ρ Oph caught an even more powerful flare with a peak luminosity of at least 10^{34} erg s^{-1} (*28*). All observations show that most Class I objects are to be highly variable in x-ray emission. Recently, a model for the large x-ray flaring activity in Class I protostars was proposed (*32*) in which closed magnetic loops connecting the stellar and disk magnetic fields get twisted as a result of rotation of the disk. Magnetic loops expand and open-field configurations develop with current sheets inside the expanding loops. Plasma is ejected that becomes sufficiently hot to emit x-rays as hard as those observed with ASCA.

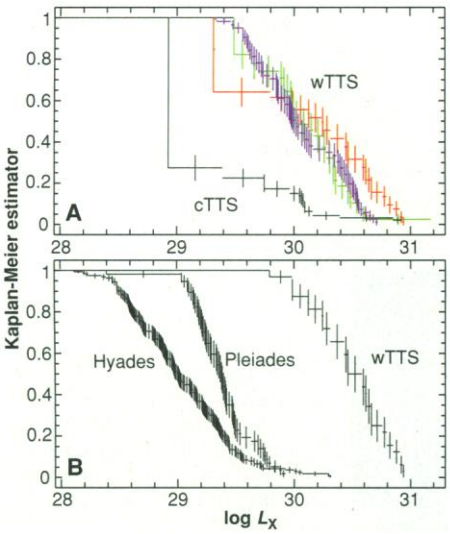

Fig. 4. (**A**) X-ray luminosity functions (XLF) for cTTS and wTTS [data from (*35*)]; plotted are Kaplan-Meier estimators (which include upper limits) versus x-ray luminosity (L_X in ergs per second), all corrected for absorption; the XLF for three wTTS groups are shown: non–x-ray–discovered wTTS (red), EO-discovered wTTS (green), and RASS-discovered wTTS (blue) are indistinguishable. (**B**) The XLF of Hyades (6×10^8 years), Pleiades (10^8 years), and RASS-detected wTTS ($\sim 10^6$ years) known before ROSAT; all data are from RASS, upper limits are excluded.

X-ray Emission from T Tauri Stars

The first systematic survey for TTS x-ray emission was conducted with EO. TTS emit ~1-keV x-rays with luminosities $\sim 10^3$ times that of the sun (*5, 33*). X-ray emission of TTS is highly variable and often shows powerful flares (*34*). Though quite a number of wTTS were discovered (*19, 20*), the total number of TTS detected with EO was fairly low because of limited sky coverage.

During RASS, all SFRs were typically surveyed with ~500-s exposure time. Hence, a large database on TTS x-ray emission now exists. Most of the well-known wTTS and only a few cTTS (because of larger absorption or lower intrinsic emission) were detected, and upper limits are available for all undetected stars (*35–39*). Deep pointed observations (Fig. 3) can detect TTS with faint x-ray emission (*26, 37, 39–41*).

To determine the x-ray emission mechanism, one can try to find correlations between x-ray emission and other stellar parameters such as rotation, but those studies suffer from low signal-to-noise in x-ray data as a result of small RASS exposure times, unresolved binaries, and other problems. However, different types of stars can be compared by using the x-ray luminosity distribution functions (XLFs).

The XLF of wTTS discovered with the EO is indistinguishable from the XLF of previously known wTTS, which were detected optically by Hα and Ca surveys (Fig. 4A). The TTS x-ray emission is compared with that of Hyades and Pleiades in Fig. 4B. The Hyades is a stellar cluster $\sim 6 \times 10^8$ years old at 45 pc, and the Pleiades cluster is $\sim 10^8$ years old and at 120 pc (*42*).

Hyades, Pleiades, wTTS and cTTS emit intrinsically different levels of x-rays, possibly because of differences in stellar rotation (*5, 35, 43*). A cTTS is locked to its disk, rotates slowly, and emits few x-rays. As soon as the disk starts to disperse, the star can continue to increase its rotation as a result of contraction and angular momentum conservation; hence, wTTS are more x-ray luminous. Stars on the MS are known to rotate more slowly than TTS, so rotation slows near the ZAMS (*44*). Most Hyades and Pleiades stars rotate slowly. This picture can explain why Pleiades stars emit less x-rays than TTS but more than Hyades stars. Our sun, with a rotation period of ~30 days, shows much less x-ray activity than TTS and ZAMS stars. However, the rotation-activity relation in TTS is not firmly established yet. A correlation between x-ray emission and rotation is hard to confirm, partly because of unresolved binaries and rotational saturation of x-ray emission, and also because x-ray emission depends on other stellar parameters such as luminosity and mass. The difference in XLF of cTTS and wTTS is seen in Taurus (*35*), Lupus (*39*), and Chamaeleon (*36*). The lifetime of circumstellar disks plays an important part in the angular momentum evolution of stars (*44*). The large number of slowly rotating stars in ZAMS clusters can be explained by stars with a long-lived disk, whereas the ultra-fast rotating ZAMS stars lost their disks early in their evolution or were born without disks (*44*). After the disk dissipates, angular momentum losses are due only to stellar winds.

Discovering Young Stars with ROSAT

The RASS was performed with a flux limit similar to typical EO pointings. Because many TTS have been discovered with EO, it is hoped that many more TTS can be found with ground-based optical follow-up observations of unidentified RASS sources. Among $\sim 10^6$ RASS sources, ~25% have stellar counterparts. To identify the optical counterpart to a RASS source, one has to obtain optical spectra of objects near the x-ray position. A star showing activity indicators like Hα or Ca H and K emission may well be the true counterpart, and if it also shows strong Li 6708 Å absorption, it may be a TTS.

About 70 Li-rich stars with spectra typical for wTTS were discovered among RASS sources in the central parts of the Taurus T association (*37*). A few additional TTS were discovered with optical follow-up observations of sources found in deep ROSAT pointed observations in Taurus (*37, 41*). Several hundred more unidentified ROSAT sources still await optical identification. On the basis of ROSAT observations, many TTS were discovered in other SFRs as well, namely in Chamaeleon (*36, 40*), ρ Oph (*24*), Lupus (*39*), and Orion (*38*). Almost all the x-ray–discovered TTS are wTTS, and most TTS discovered in these ROSAT follow-up studies are located on or close to molecular clouds. In Chamaeleon, new RASS-detected TTS (*36*) are distributed all around the clouds (Fig. 5).

In a ~300°-wide area just south of the Taurus clouds, optical follow-up observations of 111 RASS sources revealed a population of 56 Li-rich stars (*45*). There are 33 stars with Li absorption stronger or as strong as stars in the young cluster IC 2602, indicating that they are not older than $\sim 3.5 \times 10^7$ years (*46*). Some of them, however, show spectral type late F or G with Li absorption only as strong as in G-type IC 2602 stars, which are just arriving on the ZAMS. Nine other young stars are located in the λ Orionis SFR, and six of them share the typical Orion radial velocity. The remaining 12 objects have spectral types K and show Li absorption in excess of the ZAMS level, indicating that they are pre-MS stars (*46*) located in an area without molecular gas. The typical velocity dispersion in star-forming clouds is ~2 to 3 km s^{-1} (*47*), too slow for stars younger than 10^7 years to travel a distance of tens of parsec, given that 1 km s^{-1} corresponds to 1 pc in 10^6 years.

The evidence for the young age of Li-rich ROSAT source counterparts in and around Taurus is based on the Li absorption strength (*45, 46*) and on a comparison of their location in the HR diagram with evolutionary tracks (*36, 37*). These young stars may have formed locally, but there is no residual gas left over. If the gas has been blown off by a recent supernova, the space motion of the wTTS left over in this region should be indistinguishable from those in the central Taurus clouds, an idea that can be tested (*46, 48*). Alternatively, they could have formed recently in existing Taurus clouds and were ejected with high velocities.

Origin of T Tauri Stars Outside Star-Forming Clouds

It was suggested that isolated pre-MS stars were ejected from their birth clouds with high velocities (*49*). Such stars were called run-away TTS (raTTS). Because raTTS were ejected in encounters within multiple protostars, they are either single stars or close binaries. Such few-body encounters can happen early in the lifetime of a multiple protostellar system, so that the study of such encounters is also useful for determining the fraction and properties of binaries. Also, a raTTS should display a peculiar spectral energy distribution and rotation period as a result of the possible effects of the encounter, by which the raTTS was ejected, on its disk and its rotation (*49*).

If there are raTTS among the pre-MS stars south of Taurus, they should move south relative to the Taurus T association. However, for those new pre-MS stars, where the proper motion could be determined, there is no evidence for southward motion relative to the Taurus association (*48*). One pre-MS star south of Taurus, however, was identified as possibly being ejected. RXJ0511.2+1031, a single star with spectral type K7V, Hα emission, and strong Li excess above the ZAMS level (*45, 46*), is projected onto the λ Orionis star-forming cloud. If it originated in Orion, it is now moving toward Earth with a velocity of ~10 km s^{-1} relative to the Orion clouds. All the known parameters for RXJ0511.2+1031 are as expected for raTTS.

If most of the pre-MS stars found outside molecular gas were ejected raTTS, then this would indicate that the ejection rate would have to be higher than expected (*49*). For example, in Chamaeleon, there are as many pre-MS stars outside the clouds as there are inside the clouds (*36*). The discovery of many widely dispersed pre-MS stars around several star-forming clouds (*36, 38, 39, 45*) may alternatively be explained by star formation in small clouds, known as cloudlets, which may be present in turbulent molecular cloud complexes such as Orion, Taurus, or Chamaeleon (*50*). As soon as stars form in such cloudlets, the molecular gas content of these clouds disperses. Left over are small groups of a few co-moving TTS (*50*). These predictions can also be tested by observation.

Star formation according to this scenario should also produce cTTS left over from recent star formation in cloudlets and cloudlets with ongoing star formation. Although cloudlets in the vicinity of SFRs as well as at higher galactic latitudes exist

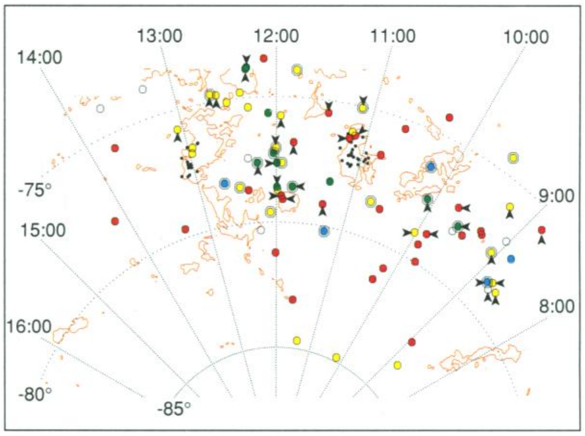

Fig. 5. The spatial distribution of ROSAT TTS in Chamaeleon (*36*). New wTTS with spectral type M are circled. Blue dots are for 10^5-year-old TTS, green dots for 10^5- to 10^6-year-old TTS, yellow dots for 10^6- to 5 × 10^6-year-old TTS, and red dots for 5 × 10^6- to 3 × 10^7-year-old TTS. Those Li-rich stars, which are marked by an arrow, show more Li in high-resolution spectra than ZAMS stars of the same spectral types (*36*). IRAS 100-μm contour lines are shown in red, and previously known cTTS as small black dots.

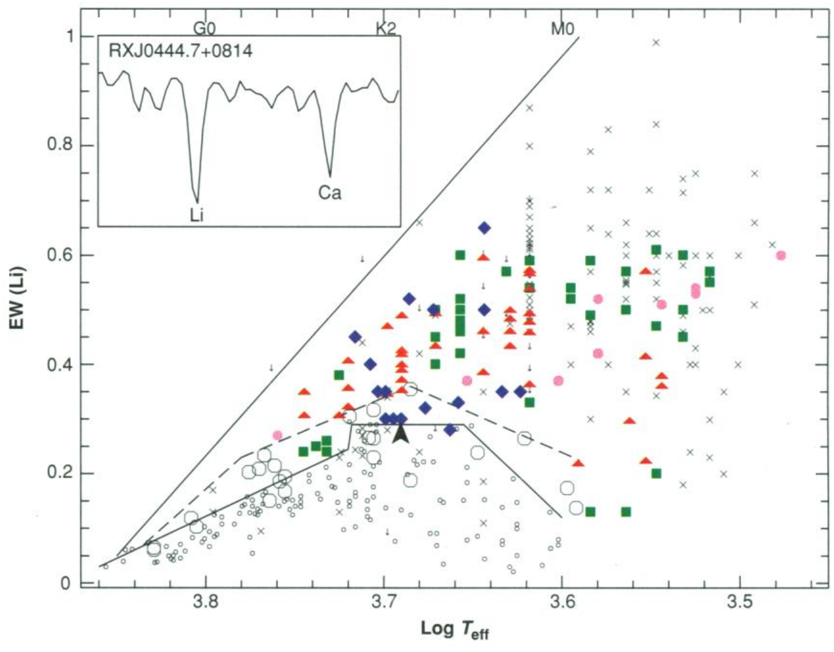

Fig. 6. Lithium equivalent width (EW) (in angstroms) versus the log of the effective temperature (in kelvin) for Pleiades (small open circles), IC 2602 stars (large open circles), all data from (*18*), high-resolution data (black crosses) for previously known bona fide TTS in central Taurus [low-resolution data (down-pointing arrows) for G- and K-type TTS as upper limits; see (*45*) for references], and new ROSAT TTS south of Taurus (blue), in Lupus (red triangles), in Chamaeleon (green), and near TW Hya (pink circles) [data from (*36, 39, 45, 54*)]. Also shown are upper envelopes to the Li equivalent widths of Pleiades (lower solid line) and IC 2602 (dashed line) stars as well as the primordial Li abundance (upper solid line). (**Inset**) A typical spectrum of pre-MS stars south of Taurus with Li and calcium absorption (*45*). The location of that star in the main diagram is indicated by an arrowhead. Stars with Li stronger than in the Pleiades and IC 2602 stars are younger than these clusters. G0, K2, and M0 are spectral types corresponding to the temperatures as indicated on the lower horizontal axis.

(51), it is not clear whether they can support star formation. These small clouds with masses typically around 10 $M_{\odot}$ may be gravitationally unbound and never form stars. Also, there are no co-moving TTS groups among outside-cloud pre-MS stars (45) for which radial velocities and proper motions are known (46, 48).

Some Li-rich stars found in follow-up observations of x-ray sources outside of clouds could be $\sim 10^8$-year-old ZAMS stars (52). Such stars should be found symmetrically south and north of the galactic plane. Because the Pleiades also show quite a spread in Li abundance and x-ray characteristics similar to TTS, the Li-rich RASS counterparts could be Pleiades-like stars.

Many late-type stars among RASS counterparts show Li absorption stronger than ZAMS stars and were claimed to be pre-MS stars (36, 38, 39, 46). It is possible to overestimate the Li equivalent width in spectra with insufficient resolution (53) resulting from blending with other nearby lines or a suppressed continuum (Fig. 6). However, many ROSAT counterparts show Li absorption, as deduced from high-resolution spectra, in excess of the ZAMS level (Fig. 6) and hence are younger. Even some young M-type stars with Li absorption were found outside the Chamaeleon clouds (36) and near TW Hya (54).

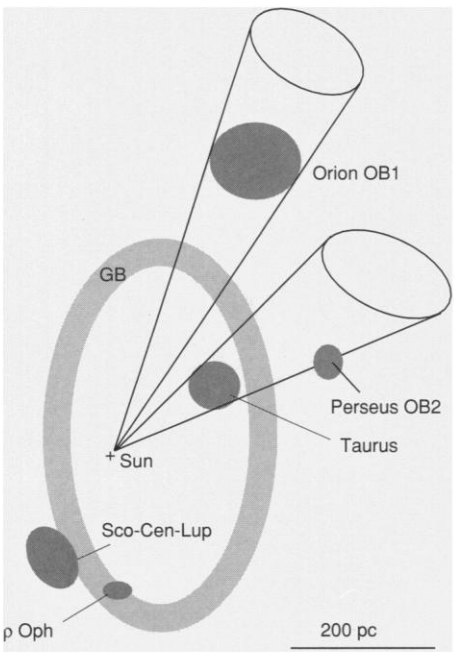

Fig. 7. Model conception of the Gould Belt (GB): The sun is located within but off-center of the belt, which is filled with $\sim 3 \times 10^7$-year-old stars. Except for the regions with ongoing star formation like ρ Oph, there are no clouds left over in the GB. The Taurus clouds are located just foreground of the belt, and the Orion and Perseus clouds are behind the belt. Scorpius-Centaurus-Lupus (Sco-Cen-Lup) and ρ Oph are in the other direction. If we observe stars in the general direction of Orion or Taurus, they can be located anywhere in the cones indicated.

Relation of the ROSAT Sources to the Gould Belt

Lithium-rich ROSAT source counterparts (39, 46) are found mostly in or projected onto the Gould Belt (GB), a band of O-, B-, and early A-type stars inclined by some 18° to the galactic plane and within 1 kiloparsec of the sun (55). Several SFRs are part of the GB (Fig. 7); however, it is not clear, whether the Taurus and Orion clouds are members of the GB, because they lie next to each other as projected onto the sky but at different distances. The origin of this structure, such as by an impact of a high-velocity cloud onto the galactic plane, is still a matter of debate (55). Several independent age estimates yield an age of up to 6×10^7 years (55). If the GB produced stars since its formation, the mean age of GB stars would be $\sim 3 \times 10^7$ years.

The optical spectra of the Li-rich ROSAT counterparts are typical for wTTS and show Li absorption at least as strong as in IC 2602 stars (39, 46), which are $\sim 3 \times 10^7$ years old. Although many Li-rich stars south of Taurus do share the typical radial velocity of TTS in central Taurus (46), the three-dimensional space motion of this population shows that it is kinematically unrelated to the Taurus T association (48). However, they are not closer than 140 pc, otherwise their magnitudes would place them below the MS, and they are not more distant, meaning much younger, because their space velocity dispersion is not small (48). All late F- and G-type stars with Li absorption at least as strong as IC 2602 stars are $\sim 3 \times 10^7$-year-old ZAMS stars, and some fraction of the K- and M-type stars indeed are pre-MS stars. These results hold for Li-rich ROSAT counterparts south of Taurus and near the Lupus clouds, but probably not for stars much more distant from star-forming clouds or outside the GB (56).

For Li-rich stars in the general direction of Orion, narrow-band Strömgren photometry was performed, which yields absolute magnitudes and, hence, individual distances for stars on or near the ZAMS (38). Stars with small Li excesses above the ZAMS level are found at distances of ~ 130 pc, foreground to the Orion clouds, whereas stars with large Li excesses lie above the ZAMS, so that no distances can be obtained with narrow-band photometry. The stars with large Li excesses appear to lie preferentially inside the Orion clouds, in the background of the GB (Fig. 7). The stars with lower Li absorption, the GB members, are distributed randomly in the studied field. In and around the Taurus clouds, the picture is similar. We see young pre-MS stars inside the clouds and more evolved ZAMS stars anywhere on the GB. However, in the direction of Taurus, we see the Taurus clouds in front of the GB (Fig. 7). In addition, there should always be a population of stars with even less Li absorption below the detection limit in most studies, namely, the $\sim 10^8$-year-old ZAMS stars. They are projected on SFRs, on the GB, and outside of the GB.

Essentially, there are three populations seen in ROSAT follow-up studies: (i) truly young K- and M-type pre-MS stars, most of which are associated with the clouds; (ii) about 3×10^7-year-old G-type ZAMS stars anywhere on the GB; and (iii) about 10^8-year-old ZAMS stars on and off the GB. The fractions of pre-MS and ZAMS stars depend on the location of these stars. There are about as many pre-MS stars located in the clouds as GB ZAMS stars (38, 46). Near clouds but still on the GB, there are about three times as many ZAMS stars as pre-MS stars, most of the Li-rich stars being members of the GB (46); and outside the GB, there are about 10 times as many ZAMS as pre-MS stars (46, 56).

Correcting the number of young stars discovered by RASS for the RASS flux limit and the x-ray emission variability of TTS, there are $\sim 10^3$ young low-mass stars in the general direction of Taurus associated with the Taurus clouds or the GB. Because there are also 29 B stars known in this area, the mass function in Taurus is consistent with a mass function of the field stars, that is, the number of stars per mass bin (57).

Implications for Star and Planet Formation

Accounting for the x-ray emission variability of TTS as well as for the flux limit and the incompleteness of RASS follow-up observations, it was concluded that there should be as many as ~ 1000 Li-rich stars in the Taurus direction (20, 37). In contrast, only about ~ 100 cTTS are known in the Taurus clouds, where this count should be fairly complete because cTTS can be easily detected by Hα and IR surveys. Even if only half of the RASS-discovered Li-rich stars really are pre-MS wTTS, this would yield a wTTS-to-cTTS ratio of 5:1. Because most wTTS are naked, this fraction also yields a good estimate of the fraction of TTS with disks. By comparing this fraction to the typical pre-MS lifetime, one can estimate the typical disk lifetime to be $\sim 3 \times 10^6$ years, which can then be interpreted as typical planet formation time scale. The average disk lifetime is small compared with the pre-MS lifetime, but obviously it varies from star to star, because some wTTS without disks appear to be quite young. The relatively large number of slowly rotating ZAMS stars shows that some disks live long enough for planets to form. The formation of the planets in our solar systems by accretion of dust and gas from the proto-solar nebula took $\sim 10^7$ years.

Large x-ray flares of Class I protostars of 10^{33} erg s^{-1} (*29*), or even more (*28*), provide radiation, which is sufficiently hard and able to penetrate large column densities and contribute to the disk ionization. Because only the outer layer of the disk can be irradiated and because the x-ray intensity is highest at small distances from the star, the outer layer in the inner disk region is ionized and may couple with the stellar or disk magnetic field. This in turn leads to enhanced mass accretion onto the star. The deeper layers of the disk are not irradiated, so planets may form (*58*).

Space-based x-ray, optical, and IR observations have improved our understanding of the formation and early stellar evolution of low-mass stars, but many questions remain. How do multiple stars form? What is the shape of the initial mass function at the very low-mass end of the star spectrum, the answer to which will help determine how many brown dwarfs there are. How do planets form, and how many stars have planets? What is the true nature, age, and origin of the large population of Li-rich ROSAT counterparts? How do protostars and TTS emit x-rays? Next-generation x-ray telescopes like the Advanced X-ray Astrophysical Facility (AXAF) and the X-ray Multiple Mirror (XMM) mission will provide sufficient angular resolution and high-throughput spectra to enable x-ray spectroscopy of TTS. Also, the next German x-ray mission, called A Broad Band Imaging X-ray All-Sky Survey (ABRIXAS), will extend the RASS to higher energies (10 keV), providing answers to some of our questions within the next decade.

REFERENCES AND NOTES

1. F. Adam, C. Lada, F. Shu, *Astrophys. J.* **312**, 788 (1987); P. André and T. Montmerle, *ibid.* **420**, 837 (1994); review by F. Shu, F. Adams, S. Lizano, *Annu. Rev. Astron. Astrophys.* **25**, 23 (1987).
2. The HR diagram is a plot of stellar luminosity versus temperature. The effective temperature (T_{eff}) of a star is equivalent to its spectral type, which can be determined from the appearance and strength of absorption lines in the spectrum of the star. The sequence of spectral types, OBAFGKM, runs from massive, hot O stars to low-mass, cold M stars. The position on the vertical axis in the HR diagram is given as luminosity Class from I for supergiants (large surface, very luminous) to VI for small subdwarfs. Each spectral type is subdivided by arabic numbers, for example a G2.5V star (such as 16 Cyg) is slightly colder than our sun (type G2V = 5780 K effective surface temperature). See Fig. 1 for an HR diagram.
3. They were first studied and recognized as being young by George Herbig and have spectral types B or A (or early F) and display emission lines (indicated by the letter e). See F. Palla and S. Stahler, *Astrophys. J.* **418**, 414 (1993); P. Thé, M. Pérez, E. van den Heuvel, Eds., *The Nature and Evolutionary Status of Herbig Ae/Be Stars*, (ASP Conf. Ser. 62, Astronomical Society of the Pacific, San Francisco, CA, 1993).
4. Magnetic fields in TTS were measured to be ~1 kG [G. Basri, G. Marcy, J. Valenti, *Astrophys. J.* **390**, 622 (1992); E. Guenther and J. Emerson, *Astron. Astrophys.* **309**, 777 (1996)].
5. F. Walter and D. Barry, in *The Sun in Time*, C. Sonett, M. Giampapa, M. Matthews, Eds. (Univ. of Arizona Press, Tucson, 1991), pp. 633–657; T. Montmerle, E. Feigelson, J. Bouvier, P. André, in *Protostars and Planets III*, E. Levy and J. Lunine, Eds. (Univ. of Arizona Press, Tucson, 1993), pp. 689–717; M. Gagné and J.-P. Caillault, *Astrophys. J.* **437**, 361 (1994).
6. A. Rydgren, D. Zak, F. Vrba, P. Chugainov, G. Zaitseva, *Astron. J.* **89**, 1015 (1984); J. Bouvier, S. Cabrit, M. Fernandez, E. Martín, J. Matthews, *Astron. Astrophys.* **272**, 176 (1993); S. Edwards *et al.*, *Astron. J.* **106**, 372 (1993); P. Choi and W. Herbst, *ibid.* **111**, 283 (1996).
7. K. Strom, S. Strom, S. Edwards, S. Cabrit, M. Skrutskie, *Astron. J.* **97**, 1451 (1989); S. Beckwith, A. Sargent, R. Chini, R. Güsten, *ibid.* **99**, 924 (1990); reviews by S. Beckwith and A. Sargent, *Nature* **383**, 139 (1996); C. R. O'Dell and S. V. W. Beckwith, *Science* **276**, 1355 (1997).
8. C. O'Dell, Z. Wen, X. Hu, *Astrophys. J.* **410**, 696 (1993); M. McCaughrean and C. O'Dell, *Astron. J.* **111**, 1996; C. Burrows *et al.*, *Astrophys. J.* **473**, 437 (1996).
9. J. Elias, *Astrophys. J.* **224**, 857 (1978); S. Kenyon, D. Dobrzycka, L. Hartmann, *Astron. J.* **108**, 1872 (1994); T. Preibisch and M. Smith, *Astron. Astrophys.*, in press. The astrometry satellite Hipparcos has measured parallaxes from which distances have been calculated. Averaging the distances of five TTS in Taurus yields 140 ± 14 pc for the distance of the Taurus association. Individual distances of the five Taurus TTS observed by Hipparcos have a signal-to-noise ratio of only 3 for the visual magnitude of 10 to 11, and the precision of the Hipparcos distance of the Herbig Ae/Be star AB Aur (visual magnitude is 7) is the best distance measured with an error of 20 pc [R. Wichmann, U. Bastian, J. Krautter, I. Jankovics, S. M. Rucinski, data presented at the European Space Agency conference on Hipparcos results, Venice, 12 to 16 May 1997].
10. S. Rucinski and J. Krautter, *Astron. Astrophys.* **121**, 217 (1983); J. Gregorio-Hetem, J. Lépine, G. Quast, C. Torres, R. de la Reza, *Astron. J.* **103**, 549 (1992).
11. A. Boss, *Astrophys. J.* **410**, 157 (1993); A. Burkert and P. Bodenheimer, *Mon. Not. R. Astron. Soc.* **264**, 798 (1993).
12. The spectral energy distribution in the range of $\lambda \simeq 2$ to ~ 25 μm can be approximated by a power law of the form $\lambda F_\lambda = \lambda^n$ (*1*).
13. The term Class 0 object denotes an even earlier evolutionary phase with strong submillimeter excess and radio emission [P. André, D. Ward-Thompson, M. Barsony, *Astrophys. J.* **406**, 122 (1993)].
14. S. Stahler, *ibid.* **274**, 822 (1983).
15. J. Najita and F. Shu, *ibid.* **429**, 808 (1994); F. Shu *et al.*, *ibid.*, p. 781; F. Shu, J. Najita, S. Ruden, S. Lizano, *ibid.*, p. 797.
16. Reviews by G. Herbig, *Adv. Astron. Astrophys* **1**, 47 (1962); I. Appenzeller and R. Mundt, *Astron. Astrophys. Rev.* **1**, 291 (1989); C. Bertout, *Annu. Rev. Astron. Astrophys.* **27**, 351 (1989).
17. G. Herbig, in *Problems of Physics and Evolution of the Universe*, L. Mirzoyan, Ed. (Academy of Science of Armenia, Erevan, 1978), pp. 171–183.
18. D. Soderblom *et al.*, *Astron. J.* **106**, 1059 (1993); S. Randich, N. Aharpour, R. Pallavicini, C. Prosser, J. Stauffer, *Astron. Astrophys.*, in press; J. Stauffer *et al.*, *Astrophys. J.* **479**, 776 (1997).
19. R. Mundt *et al.*, *Astrophys. J.* **269**, 229 (1983); K. Strom *et al.*, *ibid.* **362**, 168 (1990).
20. A wTTS either shows weak Hα emission above the continuum or emission filling in the absorption. G-type TTS generally show no Hα emission above the continuum, and emission can only be inferred by subtracting a template spectrum of an inactive star. The term naked TTS, introduced for TTS discovered by EO, reflects the interpretation that accretion has come to a halt in TTS without emission above the continuum because they no longer have a disk. Some wTTS do show far-IR or submillimeter excess emission and are not naked. A naked TTS, however, displays a blackbody spectrum like that of a normal star without any circumstellar material. Naked TTS show Hα emission filling in the absorption and are therefore wTTS [F. Walter, *Astrophys. J.* **306**, 573 (1986); ———, A. Brown, R. Mathieu, P. Myers, F. Vrba, *Astron. J.* **96**, 297 (1988)].
21. C. Bertout, G. Basri, J. Bouvier, *Astrophys. J.* **330**, 350 (1988); A. Königl, *Astrophys. J. Lett.* **370**, L39 (1991); M. Camenzind, *Rev. Mod. Astron.* **3** (1990); P. Armitage and C. Clarke, *Mon. Not. R. Astron. Soc.* **280**, 458 (1996).
22. C. Leinert *et al.*, *Astron. Astrophys.* **278**, 129 (1993); A. Ghez, G. Neugebauer, K. Matthews, *Astron. J.* **106**, 2005 (1993); M. Simon *et al.*, *Astrophys. J.* **443**, 625 (1995); review by R. Mathieu, *Annu. Rev. Astron. Astrophys.* **32**, 405 (1994).
23. F. D'Antona and I. Mazzitelli, *Astrophys. J. Suppl.* **90**, 467 (1994).
24. S. Casanova, T. Montmerle, E. Feigelson, P. André, *Astrophys. J.* **439**, 752 (1995).
25. C. Ryter, *Astrophys. Space Sci.* **236**, 285 (1996).
26. The ROSAT x-ray satellite (*59*) was launched on 1 June 1990. ROSAT is sensitive to the soft x-ray range from 0.1 to 2.4 keV (124 to 5 Å). The high-resolution imager (HRI) has ~5 arc sec spatial resolution, and the PSPCs offer sufficient spectral resolution (0.43 at 0.93 keV) for binning the x-rays into five independent energy bands. In addition, there is a wide-field camera onboard ROSAT for the extreme UV (20 to 200 eV, or 620 to 62 Å). After the RASS, which was performed with the PSPC, ROSAT has carried out many pointed observations with the PSPC and the HRI.
27. The Japanese x-ray satellite ASCA (*60*) was launched on 20 February 1993. It is equipped with four thin-foil x-ray telescopes together with charge-coupled device (CCD) cameras and gas imaging detectors and yields high spectral resolution ($E/\Delta E \simeq 50$ at 6 keV, where E is the energy of the x-ray). Its spatial resolution, between 1 and 3 arc min, is lower compared with ROSAT, and its energy range (0.5 to 10 keV or 25 to 1.2 Å) is shifted toward higher energies.
28. N. Grosso *et al.*, *Nature* **387**, 56 (1997).
29. K. Koyama, K. Hamaguchi, S. Ueno, N. Kobayashi, E. Feigelson, *Publ. Astron. Soc. Japan* **48**, 719 (1996).
30. R. Neuhäuser and T. Preibisch, *Astron. Astrophys.*, in press.
31. T. Preibisch, *ibid.*, in press.
32. M. Hayashi, K. Shibata, R. Matsumoto, *Astrophys. J.* **468**, 37 (1996).
33. W. Ku and G. Chanan, *Astrophys. J. Lett.* **234**, L59 (1979); G. Gahm, *ibid.* **242**, L163 (1980); E. Feigelson and G. Kriss, *ibid.* **248**, L35 (1981); F. Walter and L. Kuhi, *Astrophys. J.* **250**, 254 (1981).
34. T. Montmerle, L. Koch-Miramond, E. Falgarone, J. Grindlay, *Astrophys. J.* **269**, 182 (1983); F. Walter and L. Kuhi, *ibid.* **284**, 194 (1984); T. Preibisch, H. Zinnecker, J. Schmitt, *Astron. Astrophys. Lett.* **279**, L33 (1993).
35. R. Neuhäuser, M. Sterzik, J. Schmitt, R. Wichmann, J. Krautter, *Astron. Astrophys.* **297**, 381 (1995).
36. J. Alcalá *et al.*, *Astron. Astrophys. Suppl.* **114**, 109 (1995); J. Alcalá *et al.*, *Astron. Astrophys.* **319**, 184 (1997); E. Covino *et al.*, in preparation.
37. R. Neuhäuser, M. Sterzik, J. Schmitt, R. Wichmann, J. Krautter, *Astron. Astrophys.* **295**, L5 (1995); R. Wichmann *et al.*, *ibid.* **312**, 439 (1996); J. Bouvier *et al.*, *ibid.* **318**, 495 (1997).
38. J. Alcalá, L. Terranegra, R. Wichmann, C. Chavarria, J. Krautter, *Astron. Astrophys. Suppl.* **119**, 7

(1996); J. Alcalá, C. Chavarría, L. Terranegra, in preparation.
39. R. Wichmann *et al.*, *Astron. Astrophys.* **320**, 185 (1997); J. Krautter *et al.*, *ibid.*, in press; R. Wichmann, M. Sterzik, J. Krautter, A. Metanomski, W. Voges, *ibid.*, in press; R. Wichmann *et al.*, *ibid.* **320**, 185 (1997).
40. E. Feigelson, S. Casanova, T. Montmerle, J. Guibert, *Astrophys. J.* **416**, 623 (1993); D. Huenemoerder, W. Lawson, E. Feigelson, *Mon. Not. R. Astron. Soc.* **271**, 967 (1994); W. Lawson, E. Feigelson, D. Huenemoerder, *ibid.* **280**, 1071 (1996).
41. K. Strom and S. Strom, *Astrophys. J.* **424**, 237 (1994); L. Carkner, E. Feigelson, K. Koyama, T. Montmerle, N. Reid, *ibid.* **464**, 286 (1996).
42. J. Stauffer, J.-P. Caillault, M. Gagné, C. Prosser, L. Hartmann, *Astrophys. J. Suppl.* **91**, 625 (1994); R. Stern *et al.*, *Astrophys. J.* **427**, 808 (1994).
43. R. Pallavicini *et al.*, *Astrophys. J.* **248**, 279 (1981); J. Bouvier, *Astron. J.* **99**, 946 (1990).
44. J. Bouvier, M. Forestini, S. Allain, in preparation.
45. R. Neuhäuser, M. Sterzik, G. Torres, E. Martín, *Astron. Astrophys.* **299**, L13 (1995); A. Magazzù *et al.*, *Astron. Astrophys. Suppl.*, in press.
46. R. Neuhäuser, G. Torres, M. Sterzik, S. Randich, *Astron. Astrophys.*, in press.
47. B. Jones and G. Herbig, *Astron. J.* **84**, 1872 (1979); A. Gomez de Castro and R. Pudritz, *Astrophys. J.* **409**, 748 (1993).
48. S. Frink, S. Röser, R. Neuhäuser, M. Sterzik, *Astron. Astrophys.*, in press.
49. M. Sterzik, J. Alcalá, R. Neuhäuser, J. Schmitt, *ibid.* **297**, 418 (1995); M. Sterzik and R. Durisen, *ibid.* **304**, L9 (1995); P. Armitage and C. Clarke, *Mon. Not. R. Astron. Soc.*, in press.
50. E. Feigelson, *Astrophys. J.* **468**, 306 (1996).
51. B. Bok and E. Reilly, *ibid.* **105**, 255 (1947); B. Lynds, *Astrophys. J. Suppl.* **12**, 163 (1962); L. Magnani, L. Blitz, L. Mundy, *Astrophys. J.* **295**, 402 (1985).
52. G. Micela, S. Sciortino, F. Favata, *Astrophys. J.* **412**, 618 (1993); C. Briceño, L. Hartmann, J. Stauffer, M. Gagné, S. Stern, *Astron. J.* **113**, 740 (1997).
53. However, having obtained the Li strength from spectra with sufficient resolution, one has to account for the presence of an active chromosphere transition region, which will overionize Li, resulting in an apparent underabundance [E. Houdebine and J. Doyle, *Astron. Astrophys.* **302**, 861 (1995)].
54. W. Hoff *et al.*, in preparation.
55. B. Gould, *Am. J. Sci. Arts* **8**, 325 (1874); F. Comerón, J. Torra, A. Gómez, *Astron. Astrophys.* **286**, 789 (1994); review by W. Pöppel, *Fundam. Cosmic Phys.* **118** (1996).
56. F. Favata, M. Barbera, G. Micela, S. Sciortino, *Astron. Astrophys.* **277**, 428 (1993); G. Tagliaferri, G. Cutispoto, R. Pallavicini, S. Randich, L. Pasquini, *ibid.* **285**, 272 (1994); R. Jeffries, *Mon. Not. R. Astron. Soc.* **273**, 559 (1995).
57. F. Walter and W. Boyd, *Astrophys. J.* **370**, 318 (1991); G. Miller and J. Scalo, *Astrophys. J. Suppl.* **41**, 512 (1979).
58. A. Glassgold, J. Najita, J. Igea, *Astrophys. J.* **480**, 344 (1997).
59. J. Trümper, *Adv. Space Res.* **2**, 241 (1983).
60. Y. Tanaka, H. Inoue, S. Holt, *Publ. Astron. Soc. Japan* **46**, L37 (1994).
61. I thank J. Alcalá, J. Bouvier, E. Covino, W. Hoff, T. Montmerle, G. Morfill, T. Preibisch, R. Pudritz, J. Schmitt, M. Sterzik, J. Trümper, R. Wichmann, and the referees for useful discussion and providing data before publication and the Deutsche Forschungsgemeinschaft Physics of Star Formation program for financial support. The ROSAT project is supported by the Max-Planck-Gesellschaft and the German government.

Globular Clusters at Low and High Redshift

Denis Burgarella

Globular clusters form homogeneous populations of stars. On the one hand, because initial conditions are homogeneous within one cluster but vary from cluster to cluster, their study can shed light on stellar evolution processes. On the other hand, globular clusters contain the oldest known stellar population in galaxies. The study of the characteristics of globular cluster systems is one way to understand parent galaxy formation and early evolution. Unfortunately, a direct observation of the time when globular clusters and galaxies formed is still out of reach for today's telescopes, but this remains a major goal.

Globular clusters (GCs) are nearly spherical stellar systems of 10^4 to 10^6 stars orbiting around the center of the Milky Way (*1*). At first sight, the mass contained in our GC system (GCS) seems negligible compared to the rest of the galaxy. If we add up the total mass of the more than 100 known GCs, it only amounts to about 2% of the halo mass (*2*). The characteristic that makes this population so crucial resides in the age of the stars, the halo GCs contain the oldest known stars formed as part of the galaxy formation process (*2*). The study of GCS can therefore place constraints on the formation of the GCs and thereby on the formation of the Milky Way.

Extending these studies to extragalactic GCS has been difficult and only the closest ones in the local group of galaxies (such as M31 and M33) have been well studied (*3–5*). The Hubble Space Telescope (HST) and large, ground-based telescopes are extending the observing capabilities, routinely as far as the Virgo galaxy cluster (*6, 7*) and with more difficulties, to the Coma galaxy cluster (*8*). Star clusters are presently forming in galaxies, such as the magellanic clouds (*9, 10*), but they are probably less massive than the Milky Way GCs. Astronomers wonder whether young clusters similar to the Milky Way GCs are currently forming in other galaxies (*11*). If they actually do, a good place to look is in merging/interacting galaxies. Although not completely accepted (*12*), young GCs have probably been discovered by HST around the colliding galaxies NGC4038 and NGC4039 ("the Antennae") (*13*). A number of other young GCs have been found around other merging/interacting galaxies and spectroscopic observations seem to confirm this hypothesis (*14*). If we account for the difference in age, their characteristics are similar to the old GCs of our galaxy (*15*). The following chapter of this story will be to directly observe the formation of the GCs in order to understand how today's normal galaxies like the Milky Way formed.

D. Burgarella is in the Laboratoire d'Astronomie Spatiale, Traverse du Siphon, B.P. 8, 13376, Marseille CEDEX 12, France. E-mail: burgarella@astrsp-mrs.fr

The Main Sequence Turn-Off and Globular Cluster Age in the Local Group

The color-magnitude diagram (CMD) of a GC is the observational counterpart of the Hertzsprung-Russell diagram (HRD) (*16*). It is similar to a book where one can read the history of the GC. For a given GC, the location of a star in the HRD depends on its luminosity, L, and its effective temperature, T_{eff}, which in turn depends on parameters such as the evolutionary stage, the mass, the radius, and the chemical abundances of the star. The observable values corresponding to the L and T_{eff} are the magnitude (*17*) and the difference between two given magnitudes, called the color. The stars are not located at random on the CMD, rather it is like an instantaneous picture of a GC where every phase of the stellar evolution lies within a specific area usually called a sequence or a branch. The amount and quality of information gathered depends on the GC's distance and the conditions of observation such as the telescope, the detectors, the site of the telescope, and so on. In order to correctly interpret a GC's CMD, we need to (i) assume an initial mass function (IMF), $\Phi(M)$, with its characteristics, the slope α, the minimum mass, M_{min}, and the maximum mass, M_{max}, and (ii) simulate the evolution of a star and find out where it should be in the CMD after a given time Δt. The IMF is defined as the number, N, of zero-age MS (ZAMS) stars formed between M_{min} and M_{max} whose mass M_{star} is in the mass range [M_{star}, M_{star} + dM], and C is a normalization constant: